Science of Remote Sensing 7 (2023) 100075

Contents lists available at ScienceDirect

Science of Remote Sensing

journal homepage: www.sciencedirect.com/journal/science-of-remote-sensing

Estimating local-scale forest GPP in Northern Europe using Sentinel-2: Model comparisons with LUE, APAR, the plant phenology index, and a light response function

Sofia Junttila [a,*], Jonas Ardö [a], Zhanzhang Cai [a], Hongxiao Jin [a,b], Natascha Kljun [c], Leif Klemedtsson [d], Alisa Krasnova [e], Holger Lange [f], Anders Lindroth [a], Meelis Mölder [a], Steffen M. Noe [e], Torbern Tagesson [a,g], Patrik Vestin [a], Per Weslien [d], Lars Eklundh [a]

[a] Department of Physical Geography and Ecosystem Sciences, Lund University, Sölvegatan 12, SE-22362, Lund, Sweden
[b] Department of Environmental Engineering, Technical University of Denmark, Bygningstorvet 115, DK-2800, Kgs, Lyngby, Denmark
[c] Center for Environmental and Climate Science, Lund University, Sölvegatan 37, SE-22362, Lund, Sweden
[d] Department of Earth Sciences, University of Gothenburg, SE-40530, Gothenburg, Sweden
[e] Department of Plant Physiology, Institute of Agricultural and Environmental Sciences, Estonian University of Life Sciences, Fr.R. Kreutzwaldi 1, EE-51014, Tartu, Estonia
[f] Department of Biogeochemistry and Soil Quality, Division of Environment and Natural Resources, Norwegian Institute of Bioeconomy Research, Høgskoleveien 8, 1433, Ås, Norway
[g] Department of Geosciences and Natural Resource Management, University of Copenhagen, Øster Voldgade 10, DK-1350, Copenhagen, Denmark

ARTICLE INFO

Keywords:
Enhanced vegetation index 2
Gross primary production
Light response function
Plant phenology index
Sentinel-2

ABSTRACT

Northern forest ecosystems make up an important part of the global carbon cycle. Hence, monitoring local-scale gross primary production (GPP) of northern forest is essential for understanding climatic change impacts on terrestrial carbon sequestration and for assessing and planning management practices. Here we evaluate and compare four methods for estimating GPP using Sentinel-2 data in order to improve current available GPP estimates: four empirical regression models based on either the 2-band Enhanced Vegetation Index (EVI2) or the plant phenology index (PPI), an asymptotic light response function (LRF) model, and a light-use efficiency (LUE) model using the MOD17 algorithm. These approaches were based on remote sensing vegetation indices, air temperature (T_{air}), vapor pressure deficit (VPD), and photosynthetically active radiation (PAR). The models were parametrized and evaluated using in-situ data from eleven forest sites in North Europe, covering two common forest types, evergreen needleleaf forest and deciduous broadleaf forest. Most of the models gave good agreement with eddy covariance-derived GPP. The VI-based regression models performed well in evergreen needleleaf forest (R^2 = 0.69–0.78, RMSE = 1.97–2.28 g C m^{-2} d^{-1}, and NRMSE = 9–11.0%, eight sites), whereas the LRF and MOD17 performed slightly worse (R^2 = 0.65 and 0.57, RMSE = 2.49 and 2.72 g C m^{-2} d^{-1}, NRMSE = 12 and 13.0%, respectively). In deciduous broadleaf forest all models, except the LRF, showed close agreements with the observed GPP (R^2 = 0.75–0.80, RMSE = 2.23–2.46 g C m^{-2} d^{-1}, NRMSE = 11–12%, three sites). For the LRF model, R^2 = 0.57, RMSE = 3.21 g C m^{-2} d^{-1}, NRMSE = 16%. The results highlighted the necessity of improved models in evergreen needleleaf forest where the LUE approach gave poorer results., The simplest regression model using only PPI performed well beside more complex models, suggesting PPI to be a process indicator directly linked with GPP. All models were able to capture the seasonal dynamics of GPP well, but underestimation of the growing season peaks were a common issue. The LRF was the only model tending to overestimate GPP. Estimation of interannual variability in cumulative GPP was less accurate than the single-year models and will need further development. In general, all models performed well on local scale and demonstrated their feasibility for upscaling GPP in northern forest ecosystems using Sentinel-2 data.

* Corresponding author.
E-mail address: sofia.junttila@nateko.lu.se (S. Junttila).

https://doi.org/10.1016/j.srs.2022.100075
Received 3 October 2022; Received in revised form 2 December 2022; Accepted 28 December 2022
Available online 1 January 2023

1. Introduction

Accurate accounting of land-atmosphere exchange of carbon dioxide (CO_2) is essential for quantifying and understanding the global carbon cycle. Uptake of CO_2 via photosynthesis, known as gross primary production (GPP) at the ecosystem level, is a key component of the terrestrial carbon cycle (Beer et al., 2010). Boreal forest ecosystems are an important part of the global carbon cycle as they are the second largest forest ecosystem covering over 1200 million ha (Keenan et al., 2015; Tagesson et al., 2020), and contain over 30% of the global terrestrial carbon in soil and living biomass (Bradshaw and Warkentin, 2015; Pan et al., 2011). Keeling et al. (1996) have also suggested that the northern hemisphere provides a missing CO_2 sink of the global carbon cycle. Hence, monitoring GPP of northern forest is essential for understanding the climatic change impacts on terrestrial carbon sequestration.

The eddy covariance (EC) technique provides measurements of net ecosystem exchange (NEE) that can be partitioned into ecosystem respiration (ER) and GPP (Baldocchi, 2003), but to upscale CO_2 fluxes from local to regional or global levels, remote sensing-based methods are essential (Chen et al., 2010; Miettinen et al., 2021; Tramontana et al., 2015; Ueyama et al., 2013a). Remotely-sensed data offer spatially continuous information on vegetation properties and productivity related to carbon uptake over large areas but applying these data to accurately upscale carbon dynamics is still a challenge.

The accuracy of upscaled carbon flux estimates is dependent on factors such as model complexity, the choice of variables used as drivers, data quality and the representativeness of the training data set. Empirical models generally perform well for areas that have similar characteristics to training data, but fail when applied for areas or situations that are not represented in the model calibration. In addition, the choice of the drivers is a crucial step and need to be balanced between usefulness for carbon exchange estimation, availability in gridded format and sufficient data quality. Usually not all primary characteristics that effect carbon exchange (i.e., vegetation type, age, health, abiotic and biotic stress, seasonality, and phenology) may be available for large area estimation. Tramontana et al. (2015) suggests using only remotely sensed data for upscaling of GPP to avoid the uncertainty of modelled drivers, although missing of some key information might affect the accuracy of an estimate. The most common satellite-derived approaches for quantifying GPP are the light use efficiency model (LUE) (Mäkelä et al., 2008; Running et al., 2004), empirical models based on site- or ecosystem-specific relationship between EC-derived GPP and remotely sensed vegetation indices (Olofsson et al., 2008; Sims et al., 2006), and mechanistic models with remotely sensed inputs (Ryu et al., 2011; Tagesson et al., 2009). The LUE model by Monteith (1972) expresses GPP as the product of photosynthetically active radiation (PAR) incident on vegetation, the fraction of photosynthetically active radiation absorbed by the vegetation (fAPAR), and the conversion efficiency of absorbed PAR energy (ϵ). Several studies have shown that satellite-derived spectral vegetation indices have linear or near-linear relationships with fAPAR within different vegetation types and climatic conditions, and vegetation indices are therefore used as proxies of fAPAR (Fensholt et al., 2004; Olofsson et al., 2007; Running et al., 2004; Tagesson et al., 2012). The relationship between GPP and absorbed PAR (APAR, i.e. incident PAR multiplied by fAPAR) generally has an asymptotic shape at the diurnal to daily time step, but it can be considered as linear over monthly or annual periods (Falge et al., 2001; Monteith, 1977; Tagesson et al., 2015). Although a linear relationship between GPP and APAR is a widely used assumption in remote sensing–based GPP studies, several studies have also investigated nonlinear relationships to find a closer relationship between observed GPP and an explanatory variable (Gitelson et al., 2014; Noumonvi and Ferlan, 2020; Peng and Gitelson, 2011; Verma et al., 2015). Another limitation of the LUE model is the uncertainty of the light use efficiency factor (ϵ) at the landscape level, as it varies significantly among vegetation types (Turner et al., 2003) and under different types of environmental stresses (Running et al., 2004). Moreover, ϵ varies across seasons and phases of the phenological cycle causing a hysteresis in the relationship between GPP and absorbed PAR (Jenkins et al., 2007; Madani et al., 2014). To overcome the uncertainty of estimating LUE coefficient correctly and to better accommodate the detected nonlinear relationship between GPP and PAR, we investigated two nonlinear (quadratic) GPP models that rely on spectral vegetation indices.

The simplest empirical GPP models use only a spectral vegetation index such as the Normalized Difference Vegetation Index (NDVI; Tucker, 1979) or the Enhanced Vegetation Index (EVI; Huete et al., 2002) to estimate GPP. However, in boreal forests, several problems have been found with using the NDVI due to its sensitivity to snow seasonality and insensitivity to the weak canopy greenness variations of coniferous trees (Delbart et al., 2005; Jönsson et al., 2010). EVI, instead, is more responsive to leaf canopy variations in dense vegetation (Huete et al., 2002). The further developed two-band Enhanced Vegetation Index (EVI2) provides similar information on vegetation properties as EVI but only uses the red and near-infrared bands; by avoiding the blue band it is less influenced by atmospheric effects (Jiang et al., 2008). While APAR is often computed from the NDVI, several authors have found that improved dynamic range of EVI leads to generally better relationship with fAPAR (Gao et al., 2000; Huete et al., 2002; Ogutu and Dash, 2013; Xiao et al., 2004b; Zhao et al., 2018), and therefore EVI has been used in several GPP models (Peng et al., 2013; Wu et al., 2010b; Xiao et al., 2004a). There is also increasing evidence that the efficiency of EVI is related to its response to green fAPAR (or chlorophyll level fAPAR by many authors) while NDVI may be more related to canopy level fAPAR (Liu et al., 2017; Xiao et al., 2004b, 2005; Zhang et al., 2005), and that green fAPAR is superior to total fAPAR for estimating GPP (Chen et al., 2022; Zhang, 2021; Zhang et al., 2013). Moreover, the ratio of fAPAR to green fAPAR is very high in coniferous forest (Zhang et al., 2013). These reasons help explaining why EVI has been successfully used for GPP estimation across a range of ecosystems (Cai et al., 2021; Schubert et al., 2010, 2012; Sims et al., 2006; Xiao et al., 2004a).

However, EVI and EVI2 are still sensitive to the effects of snow, which is a problem when estimating carbon fluxes in seasonally snow-covered areas like boreal and artic ecosystems. To overcome this issue, the plant phenology index PPI was developed (Jin and Eklundh, 2014). PPI is a physically-based vegetation index derived from a radiative transfer model, providing a nearly linear relationship with green leaf area index (LAI), and being less sensitive to soil brightness variations than NDVI and EVI (Jin and Eklundh, 2014). Along with fAPAR, LAI is a fundamental biophysical variable for characterizing the vegetation canopy structure and predicting vegetation-atmosphere interactions, and it has been shown to explain both seasonal and spatial variations of carbon fluxes (Barr et al., 2004; Ueyama et al., 2013b; Xie et al., 2019). Abdi et al. (2019) found that PPI performed well when estimating GPP for African semi-arid ecosystems, and recent phenology studies have found that PPI is able to capture the seasonal variation of GPP over the northern hemisphere (Karkauskaite et al., 2017; Tian et al., 2021). PPI thereby provides potential for estimating GPP, especially in seasonally snow-covered forest at northern latitudes.

A physiologically realistic approach to estimate GPP that takes into account the nonlinear relationship between GPP and PAR is the asymptotic light response function (LRF) (Falge et al., 2001; Lagergren et al., 2005; Lindroth et al., 2007). The two main parameters of the LRF model, the maximum GPP under light saturation (F_{opt}; μmol CO_2 m^{-2} s^{-1}) and the initial slope of the light response function (α; μmol CO_2 μmol PAR^{-1}), can be derived from EC measurements and then spatially and temporally extrapolated in relation to spectral vegetation indices (Tagesson et al., 2017, 2021). It has been shown that the photosynthetic capacity F_{opt} is closely related to leaf nitrogen level, and the initial slope α to chlorophyll concentration (Ide et al., 2010). Because seasonal changes in nitrogen and chlorophyll content are detectable in the spectral reflectance (Moharana and Dutta, 2016; Yoder and Pettigrew-Crosby, 1995), the variation of F_{opt} and α can be assessed by

using spectral vegetation indices.

Vegetation dynamics and land cover changes on local and global scales have been traditionally monitored by satellite sensors with relatively low spatial resolutions (hundred meters to kilometers). Since the spatial resolution of a satellite-based data has been shown to be a key limitation for accurate GPP estimations (Balzarolo et al., 2019; Gelybó et al., 2013; Huang et al., 2022), the new Sentinel-2A and 2B satellites with the MultiSpectral Instrument (MSI) provide a great opportunity to study GPP in heterogeneous landscapes with up to 10 m spatial resolution. Local-scale remote sensing data may become important in assessing effects of different forest management practices. There is an ongoing debate about management options for boreal forestry (Högberg et al., 2021) considering alternatives to the traditional Nordic paradigm of clear-cutting towards continuity or other forest management options (Skytt et al., 2021, 2022). Therefore, detailed GPP estimates could be used for forest carbon inventorying and estimates of local management activities, to offset increasing CO_2 emission and thus to mitigate global warming.

Cai et al. (2021) found that Sentinel-2 and coarser MODIS (Moderate Resolution Imaging Spectroradiometer) were almost equally efficient for estimating GPP, but they and also highlighted model formulation as a necessity to improve relationships, as exemplified by the different responses to temperature and light in northern and southern Sweden. With improved data accuracy, it becomes equally important to evaluate different model types. Therefore, to make progress for local scale GPP mapping, this study focuses on utilizing high-resolution Sentinel-2 data while analyzing a variety of GPP models.

Previous studies have demonstrated the potential of remote sensing-based empirical models to estimate GPP with MODIS and Sentinel-2 data in northern peatland and forest ecosystems (Junttila et al., 2021; Schubert et al., 2010, 2012). In this paper we expand on these studies by analyzing empirical linear and nonlinear GPP models and one traditional LUE model based on Sentinel-2 data to evaluate the applicability of the different model formulations for upscaling local-scale GPP across northern boreal forest ecosystems. The models are parametrized for both forest types separately and cross-validated against EC observations, and both seasonal and interannual relationships are analyzed. We also study the influence of the environmental variables air temperature (T_{air}) and vapor pressure deficit (VPD), in order to assess their dependence on external variables. This sequence of analyses helps assessing the model selection for using Sentinel-2 data in operational environmental planning and management.

2. Materials and methods

2.1. Study sites and site-level data

The study includes eleven forest sites located in northern Europe spanning latitudes from 51.08 °N to 67.75 °N (Fig. 1, Table 1). The selection was made to develop models valid for the boreal region centered on Fennoscandia, although, some southern sites belonging to the temperate climate zone were included to enable studying also some North European deciduous broadleaf forests. Eight of the sites are evergreen needleleaf forest, and three are deciduous broadleaf forests. The EE-Jvs site in Estonia contains both conifer and broadleaf stands, but in this study the site was included in the models of deciduous broadleaf forests to increase the number of sites within that group. As can be seen from Table 1, Fennoscandian forests have rather few tree species. Due to the Gulf stream the climate is characterized by mild winters and cool summers compared to other boreal regions. The study period spanned between 2017 and 2020, though data availability varied among the sites. Gap-filled 30-min GPP data were acquired from the ICOS Carbon Portal (https://www.icos-cp.eu/data-services/about-data-portal, accessed in January 2021), from the SmartSMEAR database (Junninen et al., 2009; accessed in January 2021), or from the site principal investigators (PIs) (see Table 1).

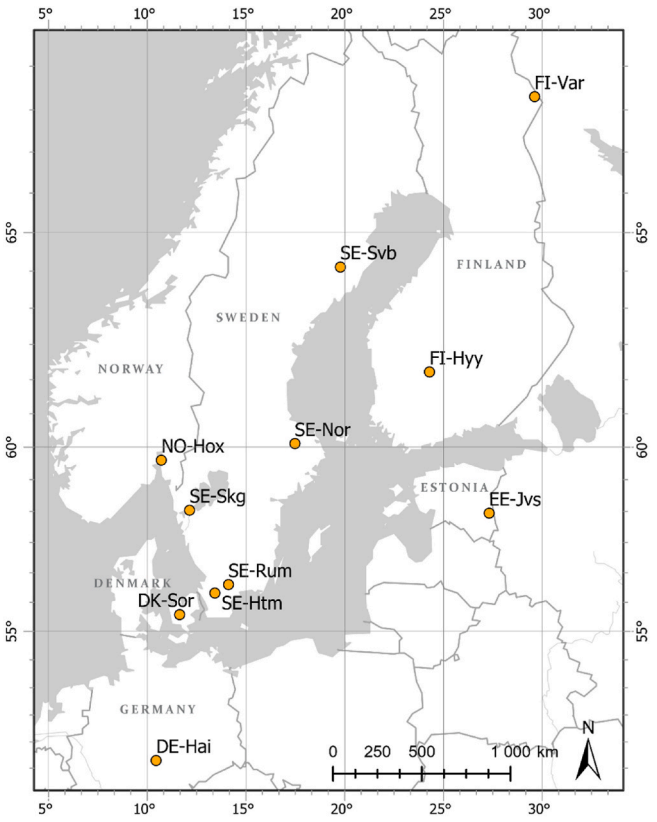

Fig. 1. Study area with locations of the eddy covariance flux measurement sites.

At the sites, auxiliary meteorological parameters, such as photosynthetically active radiation (PAR, μmol m^{-2} s^{-1}), air temperature (T_{air}, °C) and water vapor pressure deficit (VPD, hPa) are measured using standardized methodology (e.g. Rebmann et al., 2018). The 30-min measurements of GPP (GPP_{EC}), PAR, T_{air} and VPD were aggregated to daily values using a 7-day moving average with a 1-day time step to reduce the high-frequency variations in the flux data that could not be captured by the remote-sensing data due to its coarser temporal resolution.

2.2. Remote sensing data and footprint modelling

Sentinel-2 MSI data with a spatial resolution of 10 m were used to calculate the indices EVI2 and PPI. Sentinel-2 data covering each site from 2017 to 2020 were downloaded from the European Space Agency (ESA) Copernicus Sentinels Scientific Data Hub. The Sen2Cor processor (version 2.8.0) (Main-Knorn et al., 2017) was used to perform atmospheric corrections and obtain land surface reflectance and scene classification. The vegetation index EVI2 (Jiang et al., 2008) was calculated using red (ρRED) and near-infrared (ρNIR) reflectances:

$$EVI2 = 2.5 \times \frac{\rho NIR - \rho RED}{\rho NIR + 2.4 \times \rho RED + 1} \quad (1)$$

The plant phenology index PPI (Jin and Eklundh, 2014) was calculated by:

$$PPI = -K \times \ln\left(\frac{M - DVI}{M - DVI_{soil}}\right) \quad (2)$$

where DVI is the difference vegetation index (ρNIR-ρRED), DVI_{soil} is DVI for soil (an empirical value of 0.09 was used in this study (Jin and Eklundh, 2014)), M is the pixel-specific maximum DVI (estimated as the 95-percentile from the four-year time series of DVI) and K is a gain factor

Table 1
Study site characteristics and references for additional site descriptions. Forest type is based on the international Geosphere Biosphere Programme (IGBP) land cover classifications. ENF and DBF denote evergreen needleleaf forest and deciduous broadleaf forest, respectively.

Site name (Acronym)	Lat (°N)	Long (°E)	Forest type	Main tree species	GPP data	Site reference
Värriö (FI-Var)	67.75	29.61	ENF	Scots Pine (*Pinus sylvestris*)	2017–2020	Kulmala et al., (2019)
Svartberget (SE-Svb)	64.26	19.77	ENF	Scots Pine (*Pinus sylvestris*), Norway Spruce (*Picea abies*)	2018–2020	Chi et al., (2019)
Hyytiälä (FI-Hyy)	61.85	24.29	ENF	Scots Pine (*Pinus sylvestris*), Norway Spruce (*Picea abies*),	2017–2019	Kolari et al., (2009)
Norunda (SE-Nor)	60.09	17.48	ENF	Scots Pine (*Pinus sylvestris*), Norway Spruce (*Picea abies*),	2017–2020	Lindroth et al., (2018)
Hoxmark (NO-Hox)	59.67	10.72	ENF	Norway Spruce (*Picea abies*)	2018–2019	N/A
Skogaryd (SE-Skg)	58.36	12.15	ENF	Norway Spruce (*Picea abies*)	2017–2020	Lindroth et al., (2020)
Järvselja (EE-Jvs)	58.28	27.31	DBF	Birch (*Betula spec.*), Aspen (*Populus Tremula*), Scots Pine (*Pinus sylvestris*)	2017–2020	NOE et al., (2015)
Rumperöd (SE-Rum)	56.33	14.11	ENF	Norway Spruce (*Picea abies*), Scots Pine (*Pinus sylvestris*)	2017–2019	Lindroth et al., (2020)
Hyltemossa (SE-Htm)	56.10	13.42	ENF	Norway Spruce (*Picea abies*)	2017–2020	Lindroth et al., (2020)
Sorø (DK-Sor)	55.49	11.64	DBF	European Beech (*Fagus sylvatica*)	2017–2020	Pilegaard et al., (2011)
Hainich (DE-Hai)	51.08	10.45	DBF	European Beech (*Fagus sylvatica*)	2017–2019	Knohl et al., (2003)

estimated from the canopy light extinction efficiency, given by:

$$K = \frac{1}{4 \times (d_c + 0.5 \times (1 - d_c)/cos\ \theta_s))} \times \frac{1 + M}{1 - M} \quad (3)$$

where d_c is an instantaneous diffuse fraction of solar radiation at sun zenith angle θ_s (obtained from the Sentinel-2 scene metadata), computed as:

$$d_c = 0.0336 + \frac{0.0477}{\cos\ \theta_s} \quad (4)$$

In order to gap-fill and smooth the EVI2 and PPI time series, we used a combined double-logistic and spline function in the TIMESAT v.4.2.1 (Jönsson et al., 2018) software package. This method found optimal following tests of different smoothing methods available in the software package. The parameters applied in TIMESAT were: spline smoothing factor = 500, adaptation strength = 2, number of upper envelope iterations = 3. This method broadly generalizes the time-profile to a double-logistic shape, but retains flexibility to intra-seasonal variations by combining it with a spline fit. The upper envelope iterations reduce the influence of negatively biased noise due to remaining cloud or atmospheric contamination (Jönsson and Eklundh, 2002).

To enable precise matching between the Sentinel-2 data and the EC flux data, we estimated the daily EC flux footprint at each site with the two-dimensional Flux Footprint Prediction (FFP) model (Kljun et al., 2015). The model was driven by 30-min micrometeorological data (collected as part of the EC measurements) to produce daily footprint climatologies. The footprint climatologies were used to calculate weighted daily means of the EVI2 and PPI within 80% of the footprint area. The 80% flux footprint contribution is suitable to describe the main source area of the fluxes in most cases (Junttila et al., 2021; Kljun et al., 2015). The footprint modelling ensured that only pixels from the actual EC source area each day were included in the daily vegetation index averages.

2.3. MOD17 model

The widely used MOD17 algorithm (Running et al., 2004) represents a traditional LUE model (Monteith, 1972).We modified the original MOD17 algorithm to use EVI2, instead of NDVI, for estimating fAPAR. This modification was made because of previous findings supporting the use of EVI or EVI2 as a proxy for fAPAR (Liu et al., 2017; Xiao et al., 2004b; Zhang et al., 2005). Furthermore, Xiao et al. (2004a) and Xiao et al. (2004b) set EVI to be equal to fAPAR, while Zhang et al. (2013) model it as fAPARchl = 1.8*EVI-0.38. We preliminary tested both methods and concluded to use EVI2 as fAPAR due to better goodness-of-fit:

$$GPP_{MOD\ 17} = \varepsilon \times EVI2 \times PAR \quad (5)$$

where the PAR input was measured at the EC sites. Following the MOD17 algorithm, the conversion efficiency ϵ was calculated using the theoretical maximum ϵ, which is constrained with air temperature and VPD:

$$\varepsilon = \varepsilon_{max} \times T_{scalar} \times VPD_{scalar} \quad (6)$$

The restricting scalars are simple linear ramp functions of daily air temperature and VPD (Fig. 2), so that between the T_{air} and VPD limits, the scalars range from 0 (moisture and temperature conditions strongly constrain photosynthesis) and 1 (ideal conditions for photosynthesis). The maximum ε value, the T_{air} and VPD limits for both forest types were obtained from the MOD17 Biome Parameter Lookup Table (BPLUT; Running and Zhao, 2015). We applied the MOD17 scalars in all tested models to improve the model agreement with GPP_{EC} and keep the model comparison simple as the effect of T_{air} and VPD is the same in all models.

2.4. VI-based models

We investigated how the two-band Enhanced Vegetation Index (EVI2; Jiang et al., 2008) and the Plant Phenology Index (PPI; Jin and Eklundh, 2014) were related with GPP_{EC}. Due to strong literature evidence in support of EVI or EVI2 as a proxy for fAPAR (Liu et al., 2017; Ogutu and Dash, 2013; Zhang et al., 2005), we estimated APAR as the product of EVI2 and PAR. PPI, on the other hand, is closely related to LAI which is linked to GPP since it is a proxy for gross canopy chlorophyll content (Ciganda et al., 2008).

We tested nine empirical regression models fitted between GPP and PPI, EVI2 and PAR using all available site-years (see Table S1). We calculated three indicators to compare their performance: the coefficient of determination (R^2), the root-mean-square error (RMSE) and the Akaike Information Criterion (AIC). For further analysis, we selected simple linear models (Equation S1 for PPI, Equation S2 for EVI2) and two more complex models for both indices that showed a good performance in both ecosystems. We selected a multivariate linear model summing up VI and PAR (Equation S3 for both indices), a nonlinear model summing up PAR and squared EVI2 (Equation S8) and a quadratic model for the product of PPI and PAR (Equation S5).

Parametrization was done for all models and both forest ecosystems (evergreen needleleaf forest and deciduous broadleaf forest) separately. We used leave-one-out cross validation (LOOCV) with sites to evaluate the performance of the algorithm (Brovelli et al., 2008). The models were built using the training data and validated against the left out site. The procedure was repeated until all sites had served as evaluation data. After all the LOOCV runs, the average values of parameters *a*, *b* and possibly *c* (Tables S2–S8 in Supplementary Material) were applied to all sites in order to estimate GPP. Finally, the modelled GPP was multiplied with the MOD17 environmental scalar, Tscalar and VPDscalar (see Section 2.3).

We tested nine empirical regression models fitted between GPP and PPI, EVI2 and PAR using all available site-years (see Table S1). We calculated three indicators to compare their performance: the coefficient of determination (R2), the root-mean-square error (RMSE) and the

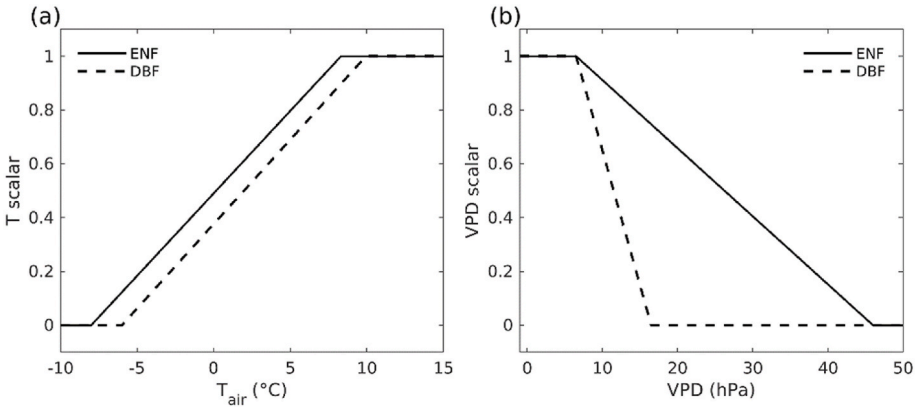

Fig. 2. The MOD17 temperature and VPD scalars for evergreen needleleaf forest and deciduous broadleaf forest.

Akaike Information Criterion (AIC). For further analysis, we selected simple linear models (Equation S1Equation S1 for PPI, Equation Equation S2 for EVI2) and two more complex models for both indices that showed a good performance in both ecosystems. We selected a multivariate linear model summing up VI and PAR (Equation S3Equation S3 for both indices), a nonlinear model summing up PAR and squared EVI2 (Equation S8Equation S8) and a quadratic model for the product of PPI and PAR (Equation S5Equation S5). Models selected for further analysis are presented in Table 2.

2.5. Light response function

To estimate GPP based on the physiologically realistic relationship between GPP_{EC} and incoming PAR at an ecosystem level, we used the asymptotic Mitscherlich light response function (LRF) following Falge et al. (2001):

$$GPP = F_{opt} \times \left(1 - e^{\frac{-\alpha \times PAR}{F_{opt}}}\right) \quad (14)$$

where F_{opt} is the optimized CO_2 uptake at light saturation or photosynthetic capacity (μmol CO_2 m^{-2} s^{-1}) and α is the quantum efficiency (μmol CO_2 μmol PAR $^{-1}$). To estimate daily values of F_{opt} and α, Equation 8 was fitted between GPP_{EC} and incoming PAR using a 7-day moving window with a 1-day time step. In order to estimate F_{opt} and α for multiple pixels, they daily time series of F_{opt} and α were coupled with EVI2 using logistic functions (Tagesson et al., 2021):

$$F_{opt} = \frac{F_{optmax}}{1 + e^{-k_F(EVI2 - b_{Fopt})}} \quad (15)$$

$$\alpha = \frac{\alpha_{max}}{1 + e^{-k_\alpha(EVI2 - b_\alpha)}} \quad (16)$$

where F_{optmax} and α_{max} are the maximum values of F_{opt} and α, k is the growth rate representing the steepness of the curve, and b is the EVI2 value of the logistic curve's midpoint. Parametrizations were done for both forest types separately with the LOOCV method. After all the LOOCV runs, the mean model parameter values (Table S6 for the evergreen needleleaf forest and Table S7 for the deciduous broadleaf forest) were applied to the sites in order to estimate F_{opt} and α with the same spatial resolution as EVI2. Upscaled F_{opt} and α enabled the computation of daily GPP (GPP_{LRF}) with a 10-m spatial resolution at the EC sites. Equations (15) and (16) were inserted into Equation (14), and GPP_{LRF} was estimated as:

$$GPP_{LRF} = \frac{F_{optmax}}{1 + e^{-k_F(EVI2 - b_F)}} \times \left(1 - e^{\frac{-\left(\frac{\alpha_{max}}{1+e^{-k_\alpha(EVI2-b_\alpha)}}\right) \times PAR}{\left(\frac{F_{optmax}}{1+e^{-k_F(EVI2-b_F)}}\right)}}\right) \quad (17)$$

Time series of daily mean GPP_{LRF} were then calculated using the same footprint climatologies as for EVI2 and PPI time series (Section 2.2). Finally, daily mean GPP_{LRF} values were multiplied with the MOD17 environmental scalars, T_{scalar} and VPD_{scalar}.

Table 2
Description of vegetation index-based empirical GPP models.

Model description	Model formula	
APAR	$APAR = EVI2 * PAR$	(7)
Linear APAR model	$GPP_{APAR\_linear} = (a * APAR + b) * T_{scalar} * VPD_{scalar}$	(8)
Linear PPI model	$GPP_{PPI\_linear} = (a * PPI + b) * T_{scalar} * VPD_{scalar}$	(9)
Multivariate linear EVI2 model	$GPP_{EVI2\_multi} = (a * EVI2 + b * PAR + c) * T_{scalar} * VPD_{scalar}$	(10)
Multivariate linear PPI model	$GPP_{PPI\_multi} = (a * PPI + b * PAR + c) * T_{scalar} * VPD_{scalar}$	(11)
Nonlinear EVI2 model	$GPP_{EVI2\_nl} = (a * EVI2^2 + b * PAR + c) * T_{scalar} * VPD_{scalar}$	(12)
Nonlinear PPI model	$GPP_{PPI\_nl} = (a * (PPI * PAR)^2 + b * PPI * PAR + c) * T_{scalar} * VPD_{scalar}$	(13)

3. Results

3.1. Relationships between GPP and explanatory variables

The vegetation indices EVI2 and PPI, and incoming solar radiation PAR together provide the main explanatory variables for all VI-based models and the MOD17 model, and EVI2 and PAR also play an important role in the LRF model.

We fitted nine regression models for GPP_{EC} based on the vegetation indices and PAR (Table S1). Several strong relationships, both linear and nonlinear, were found. PPI had especially strong quadratic relationship with GPP_{EC} in both forest types at all sites and years together: the coefficient of determination (R^2) was 0.72 for the evergreen needleleaf forest (Fig. 3c) and 0.82 for the deciduous broadleaf forest (Fig. 3d). The linear relationship was slightly weaker (R^2 was 0.62 and 0.76, respectively), yet reasonable, indicating that a linear model could also be a feasible option for PPI. For APAR, the linear and quadratic fits gave very similar results in both forest ecosystems (Fig. 3a and b). Despite the subtle improvement the quadratic model showed in comparison to the linear model, we decided to exclude a quadratic regression model for APAR due to similarity to the linear fit, and to proceed the analysis with other models.

3.2. Relationship between photosynthetic capacity and quantum efficiency with EVI2

The photosynthetic capacity (F_{opt}) showed a fairly strong logistic relationship with EVI2 for the deciduous broadleaf forest (R^2 = 0.62, Fig. 4b), while the relationship for the evergreen needleleaf forest was

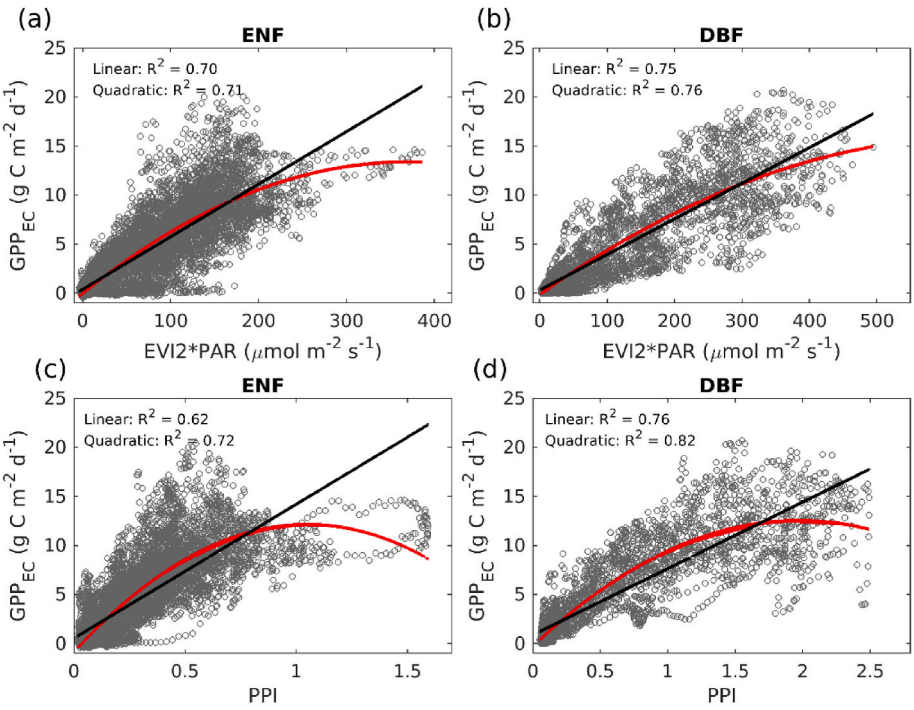

Fig. 3. Scatter plots showing the linear and quadratic regressions between GPP_{EC} and APAR (EVI2 times PAR) and PPI in both ecosystems: (a) APAR in evergreen needleleaf forest, (b) APAR in deciduous broadleaf forest, (c) PPI in evergreen needleleaf forest, and (d) PPI in deciduous broadleaf forest.

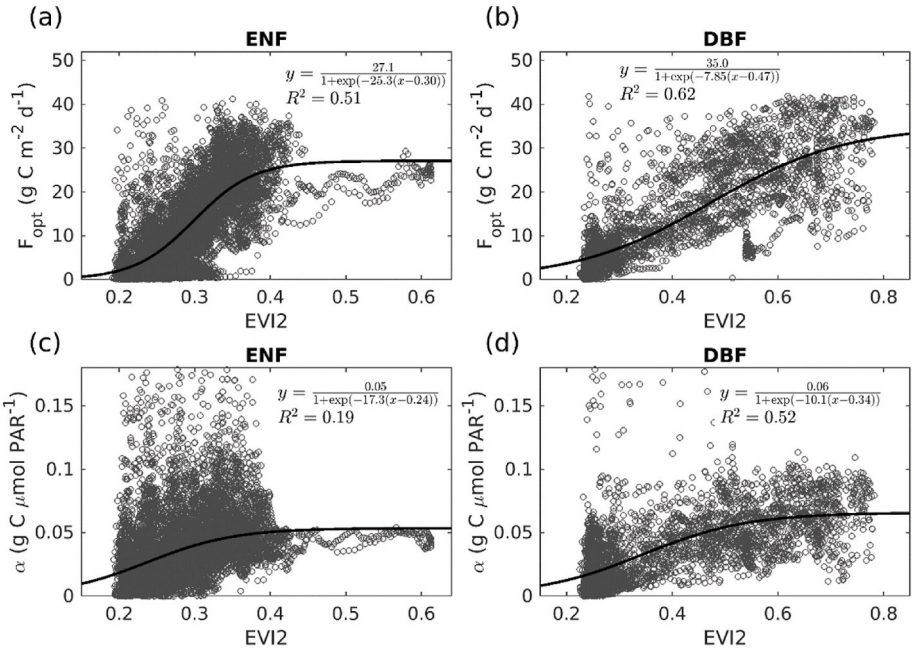

Fig. 4. Logistic fits between EVI2 and the main parameters of the LRF model: (a) photosynthetic capacity F_{opt} for evergreen needleleaf forest, (b) F_{opt} for deciduous broadleaf forest, (c) quantum efficiency α for evergreen needleleaf forest and (d) α for deciduous broadleaf forest.

slightly weaker ($R^2 = 0.51$, Fig. 4a). The other main component of the LRF model, the quantum efficiency (α), showed smaller seasonal variability, and thereby weaker relationships with EVI2 than the photosynthetic capacity. The logistic fit gave $R^2 = 0.52$ for the deciduous broadleaf forest (Fig. 4d) but only 0.19 for the evergreen needleleaf forest (Fig. 4c).

3.3. Model evaluations

The eight models were compared by evaluating daily modelled GPP against 7-day running mean GPP_{EC}. For the final evaluations, we used the models that included both T_{air} and VPD scalars from the MOD17 model. The evaluation showed that, on the whole, VI-based empirical models showed good agreement ($R^2 \geq 0.75$) with the GPP_{EC} in both forest types, same as MOD17 in deciduous broadleaf forest, whereas slightly weaker relationships were produced with the linear PPI and the

MOD17 models in evergreen needleleaf forest and LRF in both ecosystems.

When comparing the models ecosystem-wise (Table 4), the results indicate that the multivariate EVI2 model (GPP_{EVI2_multi}) gave the highest agreement ($R^2 = 0.78$, RMSE = 1.96, g C m^{-2} d^{-1}), whereas the MOD17 model performed worst ($R^2 = 0.55$, RMSE = 2.76 g C m^{-2} d^{-1}) for the evergreen needleleaf forest. Differences between the other models were small, especially all VI-based models produced 9–11% error in evergreen needleleaf forest.

For the deciduous broadleaf forest, the nonlinear PPI model gave the highest agreement and the smallest error ($R^2 = 0.80$, RMSE = 2.23 g C m^{-2} d^{-1}), although the MOD17 model presented the least bias (slope = 0.97). However, while the LRF model gave the weakest agreement with GPP_{EC} in deciduous broadleaf forest, the differences between all the other models were again very small. Overall, none of the models showed clear superiority to others at forest type-level as all of them produced 9–16% error in comparison to GPP_{EC}.

In addition, the scatter plots between for GPP_{EC} and modelled GPP indicate that most of the models underestimate the highest GPP values to some extent (Fig. 5 for ENF and Fig. 6 for DBF). The LRF model is the only model that shows systematic overestimation in both forest ecosystems. A clear saturation effect can be detected for example in $GPP_{PPI\_nonlinear}$ for both forest types (Fig. 5f for evergreen needleleaf forest and Fig. 6f for deciduous broadleaf forest), when the modelled GPP mostly stays under 15 g C m^{-2} d^{-1}, but the GPP_{EC} reaches 20 g C m^{-2} d^{-1}. The saturation effect might not be as distinct with other models, but most of them tend to underestimate highest GPP values.

It is important to realize that model fits at the site-level varied among the sites (Tables S9–S11). For example, the multivariate PPI model in SE-Svb gave the highest agreement of all sites and models ($R^2 = 0.90$, RMSE = 1.04 g C m^{-2} d^{-1}, NRMSE = 9%), whereas the greatest error (RMSE) was found in SE-Htm with the MOD17 model ($R^2 = 0.16$, RMSE = 4.44 g C m^{-2} d^{-1}, NRMSE = 22%). Some sites, like SE-Rum and EE-Jvs, showed high agreement with GPP_{EC} using all models. Time series and scatter plots of all models and individual sites are presented in Supplementary Material (Figs. S1–S8).

3.4. Estimation of annual GPP budgets

The evaluation of annual GPP budgets at forest type level revealed that underestimation was more common than an overestimation within both ecosystems (Fig. 7, Table 4). The underestimation mainly occurred at sites where the annual GPP exceeded 2000 g C m^{-2} $year^{-1}$.The goodness-of-fit statistic for modelled annual GPP and GPP_{EC} (Table 4) showed that the nonlinear PPI model produced the smallest error (R^2 = 0.68, NRMSE = 16%) for evergreen needleleaf forest, whereas other VI-based models and the LRF gave very similar annual GPP budgets (NRMSE = 17–22%), and MOD17 models showed larger error (NRMSE = 30%). Fig. 7a reveals that in evergreen needleleaf forest, the MOD17 estimates annual GPP well at sites with annual GPP less than 1000 g C m^{-2} $year^{-1}$, but underestimates sites with higher GPP, whereas the LRF model behaves in an opposite way, providing high accuracy estimates at the sites with high annual GPP, but overestimating the rest of the sites In deciduous broadleaf forest the LRF model overestimated all sites, and the MOD17 gave similar agreement as the VI-based models. The smallest error was produced with the linear and quadratic PPI models, where R^2 = 0.68 and 0.77, respectively and NRMSE = 16.5 and 16.4%, respectively.

The differences among the models within a forest type were small. For the evergreen needleleaf forest, the models produced on average 22 ± 6% error, whereas for the deciduous broadleaf forest the mean error was 22 ± 8%. Both ecosystems showed a slight tendency of underestimation of the GPP budget (the slope $\beta_1 < 1$). However, the evaluation at the site level showed greater variation among the sites and the models than the evaluation at the forest type level, as all models showed large under- and overestimations at some sites as well as very accurate estimates at other sites (see Table S12 for the summary).

4. Discussion

We compared seven empirical models and a LUE model for estimation of GPP in northern European evergreen coniferous and deciduous broadleaf forest ecosystems from Sentinel-2 data. The results showed that EVI2 and PPI-based regression models were able to capture the seasonal dynamics of GPP well and showed very similar agreement with EC-derived GPP in both forest types (Table 3, Figs. 5 and 6). The MOD17 and LRF models, on the other hand, showed more variability in results, as the LRF model gave weaker agreement in both ecosystems and the MOD17 in evergreen needleleaf forest. Although the MOD17 model performed well in deciduous broadleaf forest, its poor results in evergreen needleleaf forest reduces the value of this model for northern European forest ecosystems, which are strongly dominated by evergreen needleleaf trees. Papale et al. (2006) suggest that generally GPP_{EC} error due to the eddy covariance methodology can be around 10%. Hence, it is not possible to differentiate models whose error fall within that range (NRMSE in order of 10%), but the model have to be regarded as equally good.

The MOD17 model follows a widely used LUE approach and thus presents a linear relationship between GPP and the explanatory variables. However, several studies have revealed the difficulty in modeling interannual variability of GPP with LUE models (Wu et al., 2010a; Yuan et al., 2014). The main disadvantage of the MOD17 model is the complexity of the light use efficiency term (ε), as using a constant maximum value for each biome greatly simplifies the spatial and temporal variability in ε (Sims et al., 2006; Wang et al., 2019).We noticed that ε (i.e. the maximum ε with the restricting scalars) for deciduous broadleaf forest was suitable for our study sites. However, ε_{max} for evergreen needleleaf forest seemed suitable for the most northern sites with relatively low annual GPP, but too small for the southernmost sites where the modelled GPP was underestimated by the MOD17 model.

The maximum light use efficiency, ε_{max}, plays an important role in LUE-based models, as it defines the level of GPP, so several approaches

Table 3
Goodness-of-fit statistics for the three modelled GPP and GPP_{EC} for both forest types. ENF and DBF denote the evergreen needleleaf forest and deciduous broadleaf forest, respectively. R^2 is the coefficient of determination, RMSE is the root-mean-square error in g C m^{-2} d^{-1}, NRMSE (%) is RMSE normalized with the range (maximum–minimum) of GPP_{EC}. Slope and intercept are the ordinary least-square linear regression parameters.

Model	ENF (n = 9855)					DBF (n = 4015)				
	R^2	RMSE	NRMSE	Slope	Intercept	R^2	RMSE	NRMSE	Slope	Intercept
Linear APAR	0.76	2.02	10	0.72	1.41	0.77	2.35	11	0.69	1.00
Linear PPI	0.69	2.28	11	0.64	1.84	0.75	2.45	12	0.69	1.13
Multivariate EVI2	0.78	1.96	9	0.77	0.62	0.79	2.28	11	0.75	0.56
Multivariate PPI	0.75	2.06	10	0.77	0.53	0.78	2.33	11	0.75	0.49
Nonlinear EVI2	0.77	1.97	9	0.75	1.16	0.78	2.30	11	0.74	0.70
Nonlinear PPI	0.77	2.00	10	0.72	1.40	0.80	2.23	11	0.75	0.68
LRF	0.65	2.49	12	1.11	0.69	0.57	3.21	16	1.13	1.04
MOD17	0.57	2.72	13	0.56	0.27	0.75	2.46	12	0.97	0.61

Table 4
Goodness-of-fit statistics for annual sum GPP_{EC} against annual sums of modelled GPP for evergreen needleleaf forest (ENF) and for deciduous broadleaf forest (DBF). R^2 is the coefficient of determination, RMSE is the root-mean-square error in g C m^2 $year^{-1}$, NRMSE is RMSE normalized with the range (maximum–minimum) of GPP_{EC} in percent. β_1 is the slope and β_0 is the intercept of the ordinary least-square liner regression.

ENF (n = 27)						DBF (n = 11)				
Model	R^2	RMSE	NRMSE	β_1	β_0	R^2	RMSE	NRMSE	β_1	β_0
Linear APAR	0.63	385	17	0.49	798	0.62	292	19	0.55	544
Linear PPI	0.57	416	18	0.50	827	0.68	250	16	0.78	240
Multivariate EVI2	0.57	411	18	0.48	603	0.71	289	19	0.71	251
Multivariate PPI	0.47	457	20	0.40	702	0.64	327	22	0.67	298
Nonlinear EVI2	0.58	393	17	0.49	753	0.70	283	19	0.72	265
Nonlinear PPI	0.68	371	16	0.49	793	0.74	246	16	0.66	400
LRF	0.69	503	22	0.70	797	0.64	619	41	0.90	718
MOD17	0.51	681	30	0.30	455	0.55	318	21	0.70	621
Average	0.59	452	20	0.48	716	0.66	328	22	0.71	417
Std	0.07	95	4.2	0.10	120	0.06	113	7.5	0.09	175

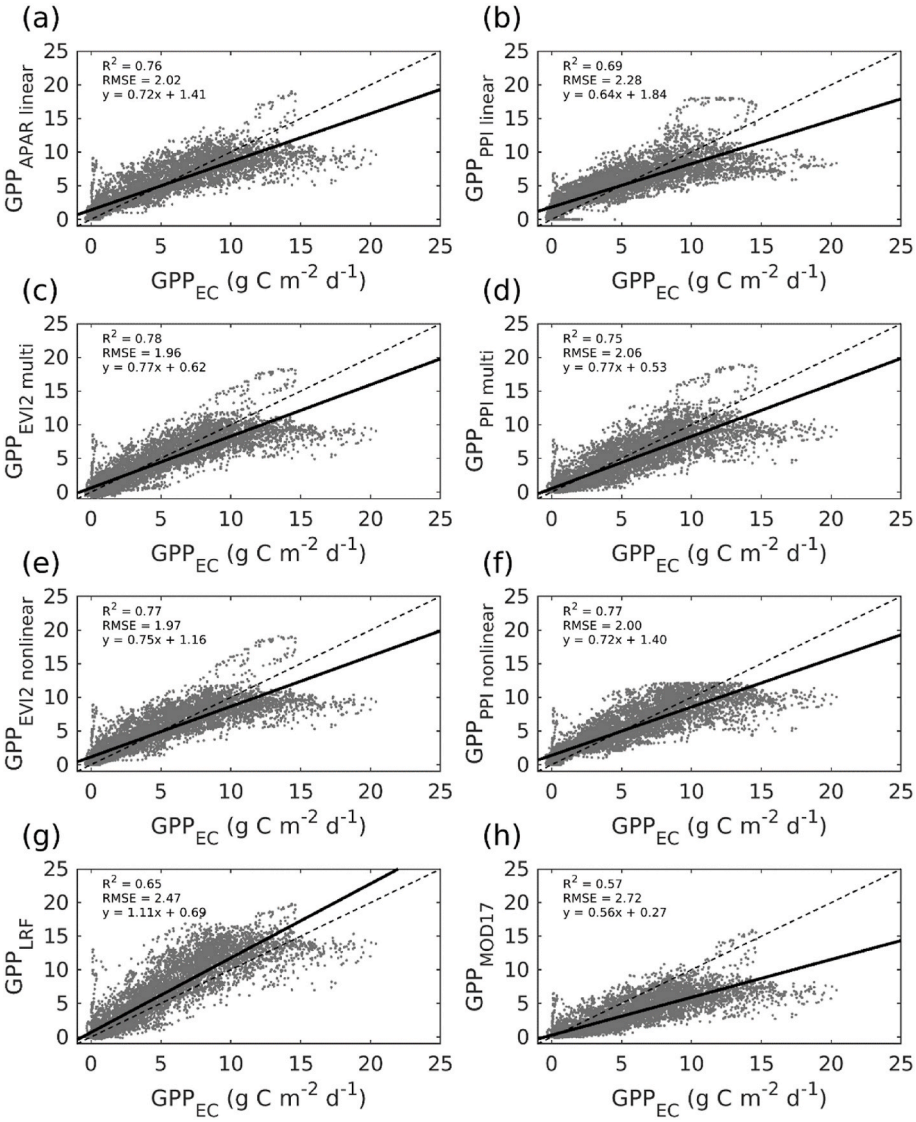

Fig. 5. Forest typelevel relationships between GPP_{EC} and each of the GPP models based on the evaluation data for evergreen needleleaf forest The dashed black line is the 1:1 line and the solid black line is the ordinary least-square linear regression line.

have been followed to overcome the difficulties to model ε_{max} correctly. Alternative way to estimate ε could be the ecosystem light-use-efficiency (eLUE; Ma et al., 2014), defined as the ratio of GPP to PAR, or to relate it with the photochemical reflectance index (PRI; Gamon et al., 1997). However, the PRI is not possible to compute using Sentinel-2 bands. Another approach would be to use the remotely sensed solar induced fluorescence (SIF) to estimate either ε or GPP directly (Mohammed et al., 2019). While current SIF products have coarse resolution, it will be generated at the ecosystem scale in future from the forthcoming Fluorescence Explorer (FLEX) satellite mission by ESA. In addition, recent

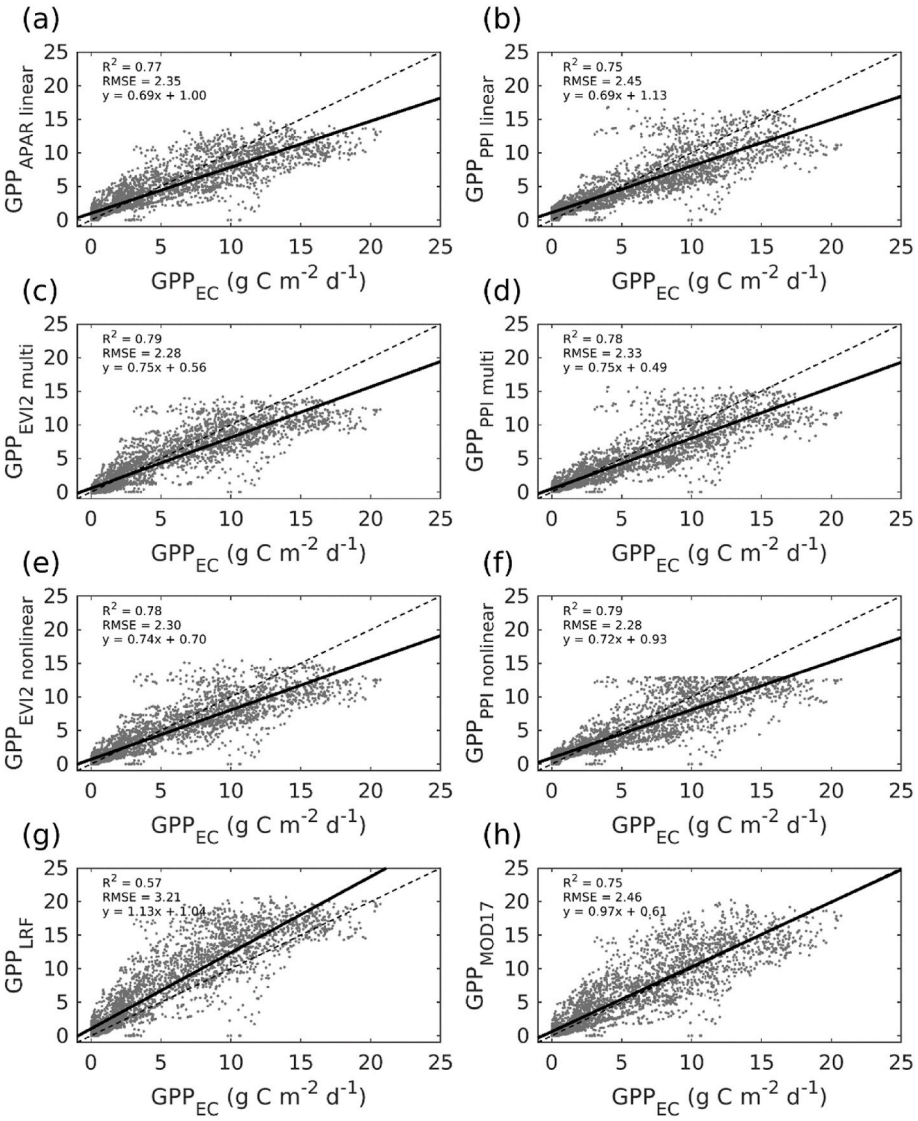

Fig. 6. Forest type-level relationships between GPP_{EC} and each of the GPP models based on the evaluation data for deciduous broadleaf forest. The dashed black line is the 1:1 line and the solid black line is the ordinary least-square linear regression line.

studies (Sun et al., 2019; Wang et al., 2020) highlight that most LUE models do not take into account the fertilization effect of increasing atmospheric CO_2 concentration, which has been noticed to enhance vegetation productivity.

In addition to MOD17 model, we presented six empirical regression models, three of them based on EVI2 and PAR, three of them based on PPI and/or PAR. These VI-based models included linear models relatively close to the MOD17 model, multivariate linear models, and nonlinear models. Nonlinear models contain the same elements as the MOD17 model but they also addresses the nonlinear relationship between GPP and PAR that has been widely observed (Falge et al., 2001; Gao et al., 2014; Lasslop et al., 2010; Turner et al., 2003). A quadratic polynomial model to estimate plant productivity has been successfully developed for agriculture ecosystems (Peng and Gitelson, 2011; Zhang et al., 2022a), whereas Wu et al. (2010b) used squared VI to increase sensitivity to high biomass situations. Here we applied similar empirical models in forest ecosystems with high agreements with EC-derived GPP. Nonlinearity in the VI-based model, as well as in the LRF model in this study, limits it scalability as the model should be applied on the same spatial and temporal scale for which it has been parameterized. Hence, re-parameterization would be needed if these models were to be applied at different spatial or temporal resolutions or if the relationship between GPP and vegetation indices change in future due to changing climate.

While the VI-based models rely on empirical regressions between vegetation indices and GPP, the LRF is a physiologically realistic approach grounded on the asymptotic relationship between EC-derived GPP and PAR (Falge et al., 2001), and it has been used to upscale GPP with EVI2 (Tagesson et al., 2021). The LRF model parameter F_{opt} and EVI2 had a strong logistic relationship especially in deciduous broadleaf forest sites (Fig. 4). The logistic relationship between α and EVI2 was also stronger for the deciduous than for the needleleaf forest, even though the relationships were in general weaker than for F_{opt}. The LRF model overestimated GPP not only during wintertime like other models, but over the whole growing season, which makes the constraining scalars essential. There is a possibility to model the environmental scalars specifically adjusted to the data, rather than using fixed functions (Tagesson et al., 2021). Independency from environmental or meteorological variables can be considered as an advantage when upscaling the results to larger areas. Hence, a future opportunity to improve the accuracy of GPP estimation is to parameterize the LRF model components F_{opt} and α with PPI instead of with EVI2. When comparing the eight models, the linear PPI model is the simplest model with the smallest number of input variables. Nevertheless, the linear PPI model performed well, particularly when considering that it does not include

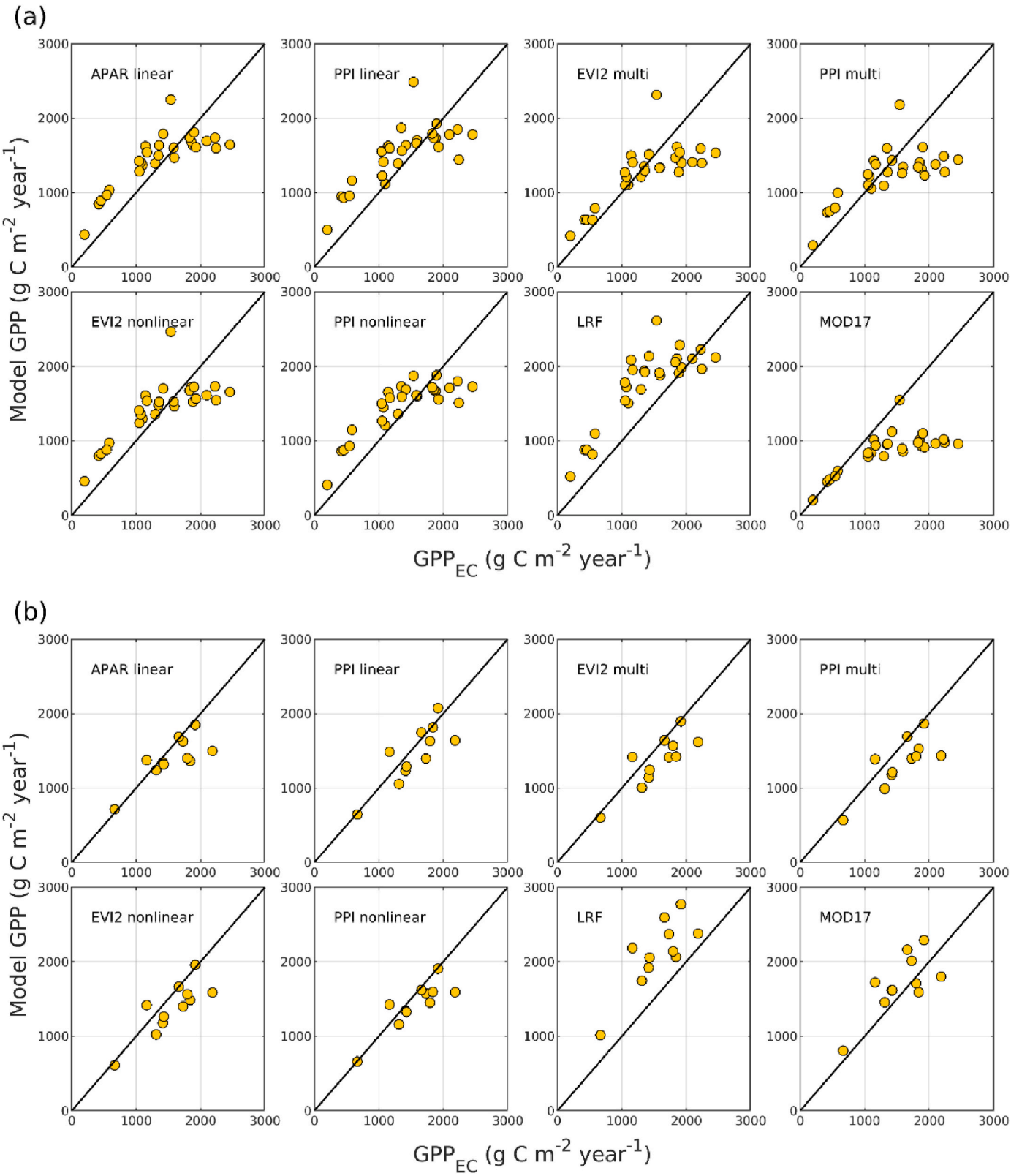

Fig. 7. Annual sum of GPP_{EC} against annual sums of modelled GPP for (a) the evergreen needleleaf forest and (b) the deciduous broadleaf forest. The black solid line is the 1:1 line.

PAR. PPI is closely linked to green LAI, which enables it to capture the canopy foliage density and a volumetric estimate of canopy chlorophyll content. Hence, PPI is less prone to saturate in dense forest canopies than e.g. NDVI, and is therefore a useful tool for estimation of GPP.

All models benefited from constraining environmental scalars to some extent. Air temperature was more important compared to VPD in both ecosystems, which is expected, given that T_{air} is a key variable regulating the photosynthetic activity in boreal forests (Mäkelä et al.,

2006). It is also possible that some part of the VPD effect is already included in the T_{scalar}, as air temperature is a component to calculate VPD. Although remote sensing-based GPP models commonly assume that VPD is able to capture the effect of drought on GPP (Running et al., 2004; Zhao and Running, 2010), several studies (Stocker et al., 2019; Tagesson et al., 2021; Yuan et al., 2014) have suggested that soil water content (SWC) is a critical variable constraining vegetation productivity, and should be taken into account in addition to VPD. Currently, distributed soil moisture data are of questionable quality, especially at high latitudes (Zhang et al., 2022b), which would complicate upscaling models built on SWC relationships.

During the summer of 2018, northwestern Europe experienced a severe drought, which increased air temperatures and induced water stress, and thus reduced GPP at several northern forest sites (Lindroth et al., 2020). In our results the effect of drought can be noticed, especially at the beech forest sites DK-Sor and DE-Hai, where EC-derived GPP drastically decreased during the 2018 growing season (Figs. S1–S8). All models were able to estimate GPP relatively well at these sites with the aid of the VPD_{scalar}. Furthermore, GPP in evergreen needleleaf forest sites was more stable over the study period, and the effect of the 2018 drought seemed to be milder in comparison to the deciduous broadleaf forest sites. An abrupt decrease and fast recovery of GPP was observed at the SE-Htm and SE-Nor sites in the peak growing season 2018, but none of the models were able to detect this (Figs. S1–S8). On the other hand, increased total GPP_{EC} was observed in SE-Nor 2018 in comparison to other years, probably due to a longer growing season. None of the models were able to capture the increased total GPP in 2018 for SE-Nor, where instead all models underestimated total GPP substantially.

Almost all models tended to underestimate GPP during the peak growing season. There are several possible explanations for that, many of them originating from cloud cover. The VI values might stay low during the peak growing season, if that period is very cloudy and good quality satellite data is not available, like we detected e.g. in SE-Htm in 2019. In general, data smoothing and gap-filling helps to overcome this issue, but it is a challenge to reach the optimal level of a VI without good quality data. Furthermore, another source of error is variation in light use efficiency with diffuse radiation during cloudy conditions (Chen et al., 2021), which may lead to GPP underestimation of >20% in coniferous forest (Choudhury, 2001). Other factors leading to underestimation are canopy clumping underestimation (Baldocchi and Harley, 1995). A further possible reason is the lack of distinction between light use efficiency differences between sunlit and shaded leaves (Chen et al., 2020; Guan et al., 2021). A final important factor is an artefact of the regression models, which suffer from the general tendency of ordinary-least-squares regression to overestimate low values and underestimate large value, and also from the assumption of errors affecting only the dependent variable Y (Riggs et al., 1978), while in reality both remotely sensed data and EC data contain considerable error. Future work may address improved statistical models for reducing this problem.

In this study, the empirical models were parameterized for two widespread forest types in northern Europe, evergreen needleleaf forest and deciduous broadleaf forest. The evergreen needleleaf forest included more EC sites creating a larger data set and thus more accurate models. Increasing the number of site-years for the deciduous forest group could help to increase variability and gain more generalized parameters. Vegetation productivity, in general, is easier to model in deciduous broadleaf forest, as this ecosystem has distinct seasonal dynamics (leaf emergence, leaf senescence and leaf fall), that can be accurately captured by remote sensing data (Yuan et al., 2014), whereas the leaf phenology in evergreen needleleaf forest is more subtle (Xiao et al., 2004a). However, general model parameterization purely based on ecosystems or land cover classes might not be able to fully explain the spatial and seasonal variability in GPP (Zheng et al., 2018). We noticed that the NO-Hox site stood out from the mature coniferous sites by its young stand age (6 and 7 years in 2018 and 2019, respectively) when studying the VI-GPP relationship. Both EVI2 and PPI gave higher values than other sites with similar peak GPP (ca. 15 g C m^{-2} day^{-1}), which can be seen in Fig. 3 as well as in Fig. 4 for the LRF parameters. To further improve the accuracy of GPP estimates, the model parameterization could be separated for spatial and seasonal variability taking into account a spatial indicator (e.g. stand age, site fertility, soil type, latitude or elevation) and different phenophases (Tagesson et al., 2017). Another factor to consider is the contribution of the GPP of the forest understory vegetation, which can play a notable role in explaining the spatial and temporal variability of forest carbon balance (Chi et al., 2021), but is not usually addressed in satellite-derived GPP models. Furthermore, variation in understory vegetation affects spectral reflectance and estimates of LAI in northern forests (Eriksson et al., 2006). Moreover, in this study, EC data from the sites were used to calibrate and validate the results in a cross-validation analysis, but with more sites and site years available, models could be evaluated against a truly independent data set to provide a more reliable evaluation.

In addition to LUE models and other data-driven models, mechanistic models have been used to estimate components of the carbon cycle. Mechanistic GPP models are generally robust as they rely on the understanding of the photosynthetic process and prescribed relationships. However, they have a considerably larger complexity than the LUE or regression based models. E.g. Ryu et al. (2011) included a large range of MODIS and other products at scales from 0.5 to 10 km, including aerosols, water vapor, land surface temperature and albedo. These products are not currently available at high spatial resolution. It is also not clear that mechanistic models always outperform empirical models, given that we still lack understanding on some processes, e.g. vegetation under drought stress (Pei et al., 2020). In future, the role of mechanistic models will likely increase, but until we have better knowledge of how to apply them at high spatial resolution there is still room for empirical models for providing users with reasonably accurate data on carbon uptake for forest planning and management.

5. Conclusions

We compared seven empirical and a light use efficiency (LUE) satellite remote sensing-based GPP models in eleven forest sites in northern Europe in 2017–2020. The models were parametrized for evergreen needleleaf forest and deciduous broadleaf forest with a leave-one-out cross validation. The GPP estimates were constrained with air temperature and vapor pressure deficit (VPD) functions in order to take into account the main environmental drivers limiting GPP. Regression models based on EVI2 or PPI were able to capture the seasonal variations in GPP derived by the eddy covariance method, while the outcome of a light response function model (LRF) and a LUE-based MOD17 model was slightly inferior. All models benefited from constraining air temperature scalars, while VPD had a significant effect on modelled GPP only in deciduous broadleaf forest. The LRF model tended to overestimate GPP over the growing seasons, indicating a need for more adjusted scalars. The simplest model, a linear regression model with PPI, performed well suggesting PPI a convenient tool for a local scale GPP estimation with reasonable accuracy yet low number of input datasets, and thus, simplifying use of remote sensing e.g. in forest management situations. However, no single model was clearly superior to the others as even though all models provided good performances, some underestimations of the peak GPP values occurred with all models. In comparison to the deciduous broadleaf forest, the needleleaf forest ecosystem had more sites spanning a climate gradient across temperate, boreal and sub-arctic areas. Hence, the magnitude of GPP and the performance of the models varied between the sites, particularly within the evergreen needleleaf forest. Especially the MOD17 model with constant biome parameters was not able to fully cover spatial variability of GPP in northern evergreen needleleaf forest, which emphasize the need for more adjustable models. We conclude that although remote sensing-based models showed great capacity to estimate local-scale seasonal GPP variations in

forest landscapes, further research is needed to better estimate inter-annual variations of GPP.

Declaration of competing interest

The authors declare that they have no known competing financial interests or personal relationships that could have appeared to influence the work reported in this paper.

Data availability

Data will be made available on request.

Acknowledgement

The study was financed by FORMAS grant 2016-01223 CarboScale to Lars Eklundh and supported by an infrastructure grant to Jonas Ardö from the Faculty of Science, Lund University. Torbern Tagesson was additionally funded by the Swedish National Space Agency (SNSA 2021-00144) and FORMAS (Dnr. 2021-00644). We also acknowledge ICOS Sweden, SITES Skogaryd station, ICOS Finland, ICOS Denmark Sorø station, and ICOS Germany Hainich station for providing GPP and environmental data. We acknowledge the European commission for free access to Copernicus Sentinel data.

Appendix A. Supplementary data

Supplementary data to this article can be found online at https://doi.org/10.1016/j.srs.2022.100075.

References

Abdi, A.M., Boke-Olén, N., Jin, H., Eklundh, L., Tagesson, T., Lehsten, V., Ardö, J., 2019. First assessment of the plant phenology index (PPI) for estimating gross primary productivity in African semi-arid ecosystems. Int. J. Appl. Earth Obs. Geoinf. 78, 249–260. https://doi.org/10.1016/j.jag.2019.01.018.

Baldocchi, D., Harley, P., 1995. Scaling carbon dioxide and water vapour exchange from leaf to canopy in a deciduous forest. II. Model testing and application. Plant Cell Environ. 18 (10), 1157–1173.

Baldocchi, D.D., 2003. Assessing the eddy covariance technique for evaluating carbon dioxide exchange rates of ecosystems: past, present and future. Global Change Biol. 9 (4), 479–492.

Balzarolo, M., Peñuelas, J., Veroustraete, F., 2019. Influence of landscape heterogeneity and spatial resolution in multi-temporal in situ and MODIS NDVI data proxies for seasonal GPP dynamics. Rem. Sens. 11 (14), 1656.

Barr, A.G., Black, T., Hogg, E., Kljun, N., Morgenstern, K., Nesic, Z., 2004. Inter-annual variability in the leaf area index of a boreal aspen-hazelnut forest in relation to net ecosystem production. Agric. For. Meteorol. 126 (3–4), 237–255.

Beer, C., Reichstein, M., Tomelleri, E., Ciais, P., Jung, M., Carvalhais, N., Bonan, G.B., 2010. Terrestrial gross carbon dioxide uptake: global distribution and covariation with climate. Science 329 (5993), 834–838.

Bradshaw, C.J., Warkentin, I.G., 2015. Global estimates of boreal forest carbon stocks and flux. Global Planet. Change 128, 24–30.

Brovelli, M.A., Crespi, M., Fratarcangeli, F., Giannone, F., Realini, E., 2008. Accuracy assessment of high resolution satellite imagery orientation by leave-one-out method. ISPRS J. Photogrammetry Remote Sens. 63 (4), 427–440. https://doi.org/10.1016/j.isprsjprs.2008.01.006.

Cai, Z., Junttila, S., Holst, J., Jin, H., Ardö, J., Ibrom, A., Eklundh, L., 2021. Modelling daily gross primary productivity with sentinel-2 data in the nordic region–comparison with data from MODIS. Rem. Sens. 13 (3), 469.

Chen, B., Arain, M.A., Chen, J.M., Wang, S., Fang, H., Liu, Z., Liu, J., 2020. Importance of shaded leaf contribution to the total GPP of Canadian terrestrial ecosystems: evaluation of MODIS GPP. J. Geophys. Res.: Biogeosciences 125 (10), e2020JG005917.

Chen, B., Ge, Q., Fu, D., Yu, G., Sun, X., Wang, S., Wang, H., 2010. A data-model fusion approach for upscaling gross ecosystem productivity to the landscape scale based on remote sensing and flux footprint modelling. Biogeosciences 7 (9), 2943–2958. https://doi.org/10.5194/bg-7-2943-2010.

Chen, S., Liu, L., Sui, L., Liu, X., 2022. Improving GPP estimates by partitioning green APAR from total APAR in two deciduous forest sites. J. For. Res. 1–13.

Chen, S., Sui, L., Liu, L., Liu, X., 2021. Effect of the partitioning of diffuse and direct APAR on GPP estimation. Rem. Sens. 14 (1), 57.

Chi, J., Nilsson, M.B., Kljun, N., Wallerman, J., Fransson, J.E.S., Laudon, H., Peichl, M., 2019. The carbon balance of a managed boreal landscape measured from a tall tower in northern Sweden. Agric. For. Meteorol. 274, 29–41. https://doi.org/10.1016/j.agrformet.2019.04.010.

Chi, J., Zhao, P., Klosterhalfen, A., Jocher, G., Kljun, N., Nilsson, M.B., Peichl, M., 2021. Forest floor fluxes drive differences in the carbon balance of contrasting boreal forest stands. Agric. For. Meteorol. 306, 108454 https://doi.org/10.1016/j.agrformet.2021.108454.

Choudhury, B.J., 2001. Estimating gross photosynthesis using satellite and ancillary data: approach and preliminary results. Remote Sens. Environ. 75 (1), 1–21.

Ciganda, V., Gitelson, A., Schepers, J., 2008. Vertical profile and temporal variation of chlorophyll in maize canopy: quantitative "crop vigor" indicator by means of reflectance-based techniques. Agron. J. 100 (5), 1409–1417. https://doi.org/10.2134/agronj2007.0322.

Delbart, N., Kergoat, L., Le Toan, T., Lhermitte, J., Picard, G., 2005. Determination of phenological dates in boreal regions using normalized difference water index. Remote Sens. Environ. 97 (1), 26–38.

Eriksson, H.M., Eklundh, L., Kuusk, A., Nilson, T., 2006. Impact of understory vegetation on forest canopy reflectance and remotely sensed LAI estimates. Remote Sens. Environ. 103 (4), 408–418.

Falge, E., Baldocchi, D., Olson, R., Anthoni, P., Aubinet, M., Bernhofer, C., Dolman, H., 2001. Gap filling strategies for defensible annual sums of net ecosystem exchange. Agric. For. Meteorol. 107 (1), 43–69.

Fensholt, R., Sandholt, I., Rasmussen, M.S., 2004. Evaluation of MODIS LAI, fAPAR and the relation between fAPAR and NDVI in a semi-arid environment using in situ measurements. Remote Sens. Environ. 91 (3), 490–507. https://doi.org/10.1016/j.rse.2004.04.009.

Gamon, J.A., Serrano, L., Surfus, J.S., 1997. The photochemical reflectance index: an optical indicator of photosynthetic radiation use efficiency across species, functional types, and nutrient levels. Oecologia 112 (4), 492–501. https://doi.org/10.1007/s004420050337.

Gao, X., Huete, A.R., Ni, W., Miura, T., 2000. Optical–biophysical relationships of vegetation spectra without background contamination. Remote Sens. Environ. 74 (3), 609–620.

Gao, Y., Yu, G., Yan, H., Zhu, X., Li, S., Wang, Q., Zhao, L., 2014. A MODIS-based photosynthetic capacity model to estimate gross primary production in northern China and the Tibetan plateau. Remote Sens. Environ. 148, 108–118.

Gelybó, G., Barcza, Z., Kern, A., Kljun, N., 2013. Effect of spatial heterogeneity on the validation of remote sensing based GPP estimations. Agric. For. Meteorol. 174, 43–53.

Gitelson, A.A., Peng, Y., Huemmrich, K.F., 2014. Relationship between fraction of radiation absorbed by photosynthesizing maize and soybean canopies and NDVI from remotely sensed data taken at close range and from MODIS 250 m resolution data. Remote Sens. Environ. 147, 108–120.

Guan, X., Chen, J.M., Shen, H., Xie, X., 2021. A modified two-leaf light use efficiency model for improving the simulation of GPP using a radiation scalar. Agric. For. Meteorol. 307, 108546.

Högberg, P., Ceder, L., Astrup, R., Binkley, D., Dalsgaard, L., Egnell, G., Kurz, W., 2021. Sustainable Boreal Forest Management Challenges and Opportunities for Climate Change Mitigation.

Huang, X., Zheng, Y., Zhang, H., Lin, S., Liang, S., Li, X., Yuan, W., 2022. High spatial resolution vegetation gross primary production product: algorithm and validation. Science of Remote Sensing 5, 100049. https://doi.org/10.1016/j.srs.2022.100049.

Huete, A., Didan, K., Miura, T., Rodriguez, E.P., Gao, X., Ferreira, L.G., 2002. Overview of the radiometric and biophysical performance of the MODIS vegetation indices. Remote Sens. Environ. 83 (1), 195–213. https://doi.org/10.1016/S0034-4257(02)00096-2.

Ide, R., Nakaji, T., Oguma, H., 2010. Assessment of canopy photosynthetic capacity and estimation of GPP by using spectral vegetation indices and the light–response function in a larch forest. Agric. For. Meteorol. 150 (3), 389–398.

Jenkins, J., Richardson, A.D., Braswell, B., Ollinger, S.V., Hollinger, D.Y., Smith, M.-L., 2007. Refining light-use efficiency calculations for a deciduous forest canopy using simultaneous tower-based carbon flux and radiometric measurements. Agric. For. Meteorol. 143 (1–2), 64–79.

Jiang, Z., Huete, A.R., Didan, K., Miura, T., 2008. Development of a two-band enhanced vegetation index without a blue band. Remote Sens. Environ. 112 (10), 3833–3845. https://doi.org/10.1016/j.rse.2008.06.006.

Jin, H., Eklundh, L., 2014. A physically based vegetation index for improved monitoring of plant phenology. Remote Sens. Environ. 152, 512–525. https://doi.org/10.1016/j.rse.2014.07.010.

Jönsson, A.M., Eklundh, L., Hellström, M., Bärring, L., Jönsson, P., 2010. Annual changes in MODIS vegetation indices of Swedish coniferous forests in relation to snow dynamics and tree phenology. Remote Sens. Environ. 114 (11), 2719–2730. https://doi.org/10.1016/j.rse.2010.06.005.

Jönsson, P., Cai, Z., Melaas, E., Friedl, M.A., Eklundh, L., 2018. A method for robust estimation of vegetation seasonality from Landsat and Sentinel-2 time series data. Rem. Sens. 10 (4), 635.

Jönsson, P., Eklundh, L., 2002. Seasonality extraction by function fitting to time-series of satellite sensor data. IEEE Trans. Geosci. Rem. Sens. 40 (8), 1824–1832. https://doi.org/10.1109/TGRS.2002.802519.

Junninen, H., Lauri, A., Keronen, P., Aalto, P., Hiltunen, V., Hari, P., Kulmala, M., 2009. Smart-SMEAR: On-Line Data Exploration and Visualization Tool for SMEAR Stations.

Junttila, S., Kelly, J., Kljun, N., Aurela, M., Klemedtsson, L., Lohila, A., Eklundh, L., 2021. Upscaling northern peatland CO2 fluxes using satellite remote sensing data. Rem. Sens. 13 (4), 818.

Karkauskaite, P., Tagesson, T., Fensholt, R., 2017. Evaluation of the plant phenology index (PPI), NDVI and EVI for start-of-season trend analysis of the northern hemisphere boreal zone. Rem. Sens. 9 (5), 485.

Keeling, R.F., Piper, S.C., Heimann, M., 1996. Global and hemispheric CO2 sinks deduced from changes in atmospheric O2 concentration. Nature 381, 218. https://doi.org/10.1038/381218a0.

Keenan, R.J., Reams, G.A., Achard, F., de Freitas, J.V., Grainger, A., Lindquist, E., 2015. Dynamics of global forest area: results from the FAO global forest resources assessment 2015. For. Ecol. Manag. 352, 9–20. https://doi.org/10.1016/j.foreco.2015.06.014.

Kljun, N., Calanca, P., Rotach, M.W., Schmid, H.P., 2015. A simple two-dimensional parameterisation for Flux Footprint Prediction (FFP). Geosci. Model Dev. (GMD) 8 (11), 3695–3713. https://doi.org/10.5194/gmd-8-3695-2015.

Knohl, A., Schulze, E.-D., Kolle, O., Buchmann, N., 2003. Large carbon uptake by an unmanaged 250-year-old deciduous forest in Central Germany. Agric. For. Meteorol. 118 (3–4), 151–167.

Kolari, P., Kulmala, L., Pumpanen, J., Launiainen, S., Ilvesniemi, H., Hari, P., Nikinmaa, E., 2009. CO2 Exchange and Component CO2 Fluxes of a Boreal Scots Pine Forest.

Kulmala, L., Pumpanen, J., Kolari, P., Dengel, S., Berninger, F., Köster, K., Bäck, J., 2019. Inter-and intra-annual dynamics of photosynthesis differ between forest floor vegetation and tree canopy in a subarctic Scots pine stand. Agric. For. Meteorol. 271, 1–11.

Lagergren, F., Eklundh, L., Grelle, A., Lundblad, M., Mölder, M., Lankreijer, H., Lindroth, A., 2005. Net primary production and light use efficiency in a mixed coniferous forest in Sweden. Plant Cell Environ. 28 (3), 412–423. https://doi.org/10.1111/j.1365-3040.2004.01280.x.

Lasslop, G., Reichstein, M., Papale, D., Richardson, A.D., Arneth, A., Barr, A., Wohlfahrt, G., 2010. Separation of net ecosystem exchange into assimilation and respiration using a light response curve approach: critical issues and global evaluation. Global Change Biol. 16 (1), 187–208. https://doi.org/10.1111/j.1365-2486.2009.02041.x.

Lindroth, A., Holst, J., Heliasz, M., Vestin, P., Lagergren, F., Biermann, T., Mölder, M., 2018. Effects of low thinning on carbon dioxide fluxes in a mixed hemiboreal forest. Agric. For. Meteorol. 262, 59–70.

Lindroth, A., Holst, J., Linderson, M.-L., Aurela, M., Biermann, T., Heliasz, M., Klemedtsson, L., 2020. Effects of drought and meteorological forcing on carbon and water fluxes in Nordic forests during the dry summer of 2018. Philosophical Transactions of the Royal Society B 375 (1810), 20190516.

Lindroth, A., Lund, M., Nilsson, M., Aurela, M., Christensen, T.R., Laurila, T., StröM, L., 2007. Environmental controls on the CO2 exchange in north European mires. Tellus B 59 (5), 812–825.

Liu, Z., Wu, C., Peng, D., Wang, S., Gonsamo, A., Fang, B., Yuan, W., 2017. Improved modeling of gross primary production from a better representation of photosynthetic components in vegetation canopy. Agric. For. Meteorol. 233, 222–234.

Ma, X., Huete, A., Yu, Q., Restrepo-Coupe, N., Beringer, J., Hutley, L.B., Eamus, D., 2014. Parameterization of an ecosystem light-use-efficiency model for predicting savanna GPP using MODIS EVI. Remote Sens. Environ. 154, 253–271. https://doi.org/10.1016/j.rse.2014.08.025.

Madani, N., Kimball, J.S., Affleck, D.L., Kattge, J., Graham, J., Van Bodegom, P.M., Running, S.W., 2014. Improving ecosystem productivity modeling through spatially explicit estimation of optimal light use efficiency. J. Geophys. Res.: Biogeosciences 119 (9), 1755–1769.

Main-Knorn, M., Pflug, B., Louis, J., Debaecker, V., Müller-Wilm, U., Gascon, F., 2017. Sen2Cor for sentinel-2. In: Proc. SPIE 10427, Image and Signal Processing for Remote Sensing XXIII, p. 1042704. https://doi.org/10.1117/12.2278218.

Mäkelä, A., Kolari, P., Karimäki, J., Nikinmaa, E., Perämäki, M., Hari, P., 2006. Modelling five years of weather-driven variation of GPP in a boreal forest. Agric. For. Meteorol. 139 (3), 382–398. https://doi.org/10.1016/j.agrformet.2006.08.017.

Mäkelä, A., Pulkkinen, M., Kolari, P., Lagergren, F., Berbigier, P., Lindroth, A., Hari, P., 2008. Developing an empirical model of stand GPP with the LUE approach: analysis of eddy covariance data at five contrasting conifer sites in Europe. Global Change Biol. 14 (1), 92–108. https://doi.org/10.1111/j.1365-2486.2007.01463.x.

Miettinen, J., Carlier, S., Häme, L., Mäkelä, A., Minunno, F., Penttilä, J., Seitsonen, L., 2021. Demonstration of large area forest volume and primary production estimation approach based on Sentinel-2 imagery and process based ecosystem modelling. Int. J. Rem. Sens. 42 (24), 9467–9489.

Mohammed, G.H., Colombo, R., Middleton, E.M., Rascher, U., van der Tol, C., Nedbal, L., Meroni, M., 2019. Remote sensing of solar-induced chlorophyll fluorescence (SIF) in vegetation: 50 years of progress. Remote Sens. Environ. 231, 111177.

Moharana, S., Dutta, S., 2016. Spatial variability of chlorophyll and nitrogen content of rice from hyperspectral imagery. ISPRS J. Photogrammetry Remote Sens. 122, 17–29. https://doi.org/10.1016/j.isprsjprs.2016.09.002.

Monteith, J.L., 1972. Solar radiation and productivity in tropical ecosystems. J. Appl. Ecol. 9 (3), 747–766. https://doi.org/10.2307/2401901.

Monteith, J.L., 1977. Climate and the efficiency of crop production in Britain. Philos. Trans. R. Soc. Lond. B Biol. Sci. 281 (980), 277–294.

Noe, S.M., Niinemets, Ü., Krasnova, A., Krasnov, D., Motallebi, A., Kängsepp, V., Mirme, S., 2015. SMEAR Estonia: perspectives of a large-scale forest ecosystem–atmosphere research infrastructure. Metsanduslikud uurimused 63 (1), 56–84.

Noumonvi, K.D., Ferlan, M., 2020. Empirical vs. light-use efficiency modelling for estimating carbon fluxes in a mid-succession ecosystem developed on abandoned karst grassland. PLoS One 15 (8), e0237351. https://doi.org/10.1371/journal.pone.0237351.

Ogutu, B.O., Dash, J., 2013. An algorithm to derive the fraction of photosynthetically active radiation absorbed by photosynthetic elements of the canopy (FAPAR ps) from eddy covariance flux tower data. New Phytol. 197 (2), 511–523.

Olofsson, P., Eklundh, L., Lagergren, F., Jönsson, P., Lindroth, A., 2007. Estimating net primary production for Scandinavian forests using data from Terra/MODIS. Adv. Space Res. 39 (1), 125–130. https://doi.org/10.1016/j.asr.2006.02.031.

Olofsson, P., Lagergren, F., Lindroth, A., Lindström, J., Klemedtsson, L., Kutsch, W., Eklundh, L., 2008. Towards operational remote sensing of forest carbon balance across Northern Europe. Biogeosciences 5 (3), 817–832. https://doi.org/10.5194/bg-5-817-2008.

Pan, Y., Birdsey, R.A., Fang, J., Houghton, R., Kauppi, P.E., Kurz, W.A., Hayes, D., 2011. A large and persistent carbon sink in the world's forests. Science 333 (6045), 988–993. https://doi.org/10.1126/science.1201609.

Papale, D., Reichstein, M., Aubinet, M., Canfora, E., Bernhofer, C., Kutsch, W., Vesala, T., 2006. Towards a standardized processing of Net Ecosystem Exchange measured with eddy covariance technique: algorithms and uncertainty estimation. Biogeosciences 3 (4), 571–583.

Pei, Y., Dong, J., Zhang, Y., Yang, J., Zhang, Y., Jiang, C., Xiao, X., 2020. Performance of four state-of-the-art GPP products (VPM, MOD17, BESS and PML) for grasslands in drought years. Ecol. Inf. 56, 101052.

Peng, Y., Gitelson, A.A., 2011. Application of chlorophyll-related vegetation indices for remote estimation of maize productivity. Agric. For. Meteorol. 151 (9), 1267–1276. https://doi.org/10.1016/j.agrformet.2011.05.005.

Peng, Y., Gitelson, A.A., Sakamoto, T., 2013. Remote estimation of gross primary productivity in crops using MODIS 250 m data. Remote Sens. Environ. 128, 186–196.

Pilegaard, K., Ibrom, A., Courtney, M.S., Hummelshøj, P., Jensen, N.O., 2011. Increasing net CO2 uptake by a Danish beech forest during the period from 1996 to 2009. Agric. For. Meteorol. 151 (7), 934–946.

Rebmann, C., Aubinet, M., Schmid, H., Arriga, N., Aurela, M., Burba, G., Franz, D., 2018. ICOS eddy covariance flux-station site setup: a review. Int. Agrophys. 32 (4), 471–494. https://doi.org/10.1515/intag-2017-0044.

Riggs, D.S., Guarnieri, J.A., Addelman, S., 1978. Fitting straight lines when both variables are subject to error. Life Sci. 22 (13–15), 1305–1360.

Running, S.W., Nemani, R.R., Heinsch, F.A., Zhao, M., Reeves, M., Hashimoto, H., 2004. A continuous satellite-derived measure of global terrestrial primary production. Bioscience 54 (6), 547–560. https://doi.org/10.1641/0006-3568(2004)054 [0547:ACSMOG]2.0.CO;2.

Running, S.W., Zhao, M., 2015. Daily GPP and Annual NPP (MOD17A2/A3) Products NASA Earth Observing System MODIS Land Algorithm. MOD17 User's Guide, pp. 1–28, 2015.

Ryu, Y., Baldocchi, D.D., Kobayashi, H., van Ingen, C., Li, J., Black, T.A., Roupsard, O., 2011. Integration of MODIS land and atmosphere products with a coupled-process model to estimate gross primary productivity and evapotranspiration from 1 km to global scales. Global Biogeochem. Cycles 25 (4). https://doi.org/10.1029/2011GB004053.

Schubert, P., Eklundh, L., Lund, M., Nilsson, M., 2010. Estimating northern peatland CO2 exchange from MODIS time series data. Remote Sens. Environ. 114 (6), 1178–1189. https://doi.org/10.1016/j.rse.2010.01.005.

Schubert, P., Lagergren, F., Aurela, M., Christensen, T., Grelle, A., Heliasz, M., Eklundh, L., 2012. Modeling GPP in the Nordic forest landscape with MODIS time series data—comparison with the MODIS GPP product. Remote Sens. Environ. 126 (Suppl. C), 136–147. https://doi.org/10.1016/j.rse.2012.08.005.

Sims, D.A., Rahman, A.F., Cordova, V.D., El-Masri, B.Z., Baldocchi, D.D., Flanagan, L.B., Xu, L., 2006. On the use of MODIS EVI to assess gross primary productivity of North American ecosystems. J. Geophys. Res.: Biogeosciences 111 (G4). https://doi.org/10.1029/2006JG000162.

Skytt, T., Englund, G., Jonsson, B.-G., 2021. Climate mitigation forestry—temporal trade-offs. Environ. Res. Lett. 16 (11), 114037 https://doi.org/10.1088/1748-9326/ac30fa.

Skytt, T., Englund, G., Jonsson, B.-G., 2022. Reply to Comment on 'Climate mitigation forestry—temporal trade-offs. Environ. Res. Lett. 17 (4), 048002 https://doi.org/10.1088/1748-9326/ac57e7.

Stocker, B.D., Zscheischler, J., Keenan, T.F., Prentice, I.C., Seneviratne, S.I., Peñuelas, J., 2019. Drought impacts on terrestrial primary production underestimated by satellite monitoring. Nat. Geosci. 12 (4), 264–270. https://doi.org/10.1038/s41561-019-0318-6.

Sun, Z., Wang, X., Zhang, X., Tani, H., Guo, E., Yin, S., Zhang, T., 2019. Evaluating and comparing remote sensing terrestrial GPP models for their response to climate variability and CO2 trends. Sci. Total Environ. 668, 696–713. https://doi.org/10.1016/j.scitotenv.2019.03.025.

Tagesson, T., Ardö, J., Cappelaere, B., Kergoat, L., Abdi, A., Horion, S., Fensholt, R., 2017. Modelling spatial and temporal dynamics of gross primary production in the Sahel from earth-observation-based photosynthetic capacity and quantum efficiency. Biogeosciences 14 (5), 1333–1348. https://doi.org/10.5194/bg-14-1333-2017.

Tagesson, T., Fensholt, R., Cropley, F., Guiro, I., Horion, S., Ehammer, A., Ardö, J., 2015. Dynamics in carbon exchange fluxes for a grazed semi-arid savanna ecosystem in West Africa. Agric. Ecosyst. Environ. 205, 15–24. https://doi.org/10.1016/j.agee.2015.02.017.

Tagesson, T., Mastepanov, M., Tamstorf, M.P., Eklundh, L., Schubert, P., Ekberg, A., Ström, L., 2012. High-resolution satellite data reveal an increase in peak growing season gross primary production in a high-Arctic wet tundra ecosystem 1992–2008. Int. J. Appl. Earth Obs. Geoinf. 18 (Suppl. C), 407–416. https://doi.org/10.1016/j.jag.2012.03.016.

Tagesson, T., Schurgers, G., Horion, S., Ciais, P., Tian, F., Brandt, M., Olin, S., 2020. Recent divergence in the contributions of tropical and boreal forests to the terrestrial carbon sink. Nature Ecology & Evolution 4 (2), 202–209.

Tagesson, T., Smith, B., Löfgren, A., Rammig, A., Eklundh, L., Lindroth, A., 2009. Estimating net primary production of Swedish forest landscapes by combining

mechanistic modeling and remote sensing. AMBIO A J. Hum. Environ. 38 (6), 316–324. https://doi.org/10.1579/08-A-513.1.
Tagesson, T., Tian, F., Schurgers, G., Horion, S., Scholes, R., Ahlström, A., Ardö, A., Moreno, A., Madani, N., Olin, S., Fensholt, R., 2021. A physiology-based Earth observation model indicates stagnation in the global gross primary production during recent decades. Global Change Biology. 27 (4), 836–854. https://doi.org/10.1111/gcb.15424.
Tian, F., Cai, Z., Jin, H., Hufkens, K., Scheifinger, H., Tagesson, T., Ivits, E., 2021. Calibrating vegetation phenology from Sentinel-2 using eddy covariance, PhenoCam, and PEP725 networks across Europe. Remote Sens. Environ. 260, 112456.
Tramontana, G., Ichii, K., Camps-Valls, G., Tomelleri, E., Papale, D., 2015. Uncertainty analysis of gross primary production upscaling using Random Forests, remote sensing and eddy covariance data. Remote Sens. Environ. 168, 360–373. https://doi.org/10.1016/j.rse.2015.07.015.
Tucker, C.J., 1979. Red and photographic infrared linear combinations for monitoring vegetation. Remote Sens. Environ. 8 (2), 127–150. https://doi.org/10.1016/0034-4257(79)90013-0.
Turner, D.P., Urbanski, S., Bremer, D., Wofsy, S.C., Meyers, T., Gower, S.T., Gregory, M., 2003. A cross-biome comparison of daily light use efficiency for gross primary production. Global Change Biol. 9 (3), 383–395. https://doi.org/10.1046/j.1365-2486.2003.00573.x.
Ueyama, M., Ichii, K., Iwata, H., Euskirchen, E.S., Zona, D., Rocha, A.V., Oechel, W.C., 2013a. Upscaling terrestrial carbon dioxide fluxes in Alaska with satellite remote sensing and support vector regression. J. Geophys. Res.: Biogeosciences 118 (3), 1266–1281. https://doi.org/10.1002/jgrg.20095.
Ueyama, M., Iwata, H., Harazono, Y., Euskirchen, E.S., Oechel, W.C., Zona, D., 2013b. Growing season and spatial variations of carbon fluxes of Arctic and boreal ecosystems in Alaska (USA). Ecol. Appl. 23 (8), 1798–1816. https://doi.org/10.1890/11-0875.1.
Verma, M., Friedl, M.A., Law, B.E., Bonal, D., Kiely, G., Black, T.A., D'Odorico, P., 2015. Improving the performance of remote sensing models for capturing intra- and inter-annual variations in daily GPP: an analysis using global FLUXNET tower data. Agric. For. Meteorol. 214–215, 416–429. https://doi.org/10.1016/j.agrformet.2015.09.005.
Wang, S., Garcia, M., Bauer-Gottwein, P., Jakobsen, J., Zarco-Tejada, P.J., Bandini, F., Ibrom, A., 2019. High spatial resolution monitoring land surface energy, water and CO2 fluxes from an Unmanned Aerial System. Remote Sens. Environ. 229, 14–31.
Wang, S., Zhang, Y., Ju, W., Chen, J.M., Ciais, P., Cescatti, A., Peñuelas, J., 2020. Recent global decline of CO_2 fertilization effects on vegetation photosynthesis. Science 370 (6522), 1295–1300. https://doi.org/10.1126/science.abb7772.
Wu, C., Munger, J.W., Niu, Z., Kuang, D., 2010a. Comparison of multiple models for estimating gross primary production using MODIS and eddy covariance data in Harvard Forest. Remote Sens. Environ. 114 (12), 2925–2939.
Wu, C., Niu, Z., Gao, S., 2010b. Gross primary production estimation from MODIS data with vegetation index and photosynthetically active radiation in maize. J. Geophys. Res. Atmos. 115 (D12).
Xiao, X., Hollinger, D., Aber, J., Goltz, M., Davidson, E.A., Zhang, Q., Moore, B., 2004a. Satellite-based modeling of gross primary production in an evergreen needleleaf forest. Remote Sens. Environ. 89 (4), 519–534. https://doi.org/10.1016/j.rse.2003.11.008.
Xiao, X., Zhang, Q., Braswell, B., Urbanski, S., Boles, S., Wofsy, S., Ojima, D., 2004b. Modeling gross primary production of temperate deciduous broadleaf forest using satellite images and climate data. Remote Sens. Environ. 91 (2), 256–270.
Xiao, X., Zhang, Q., Hollinger, D., Aber, J., Moore III, B., 2005. Modeling gross primary production of an evergreen needleleaf forest using MODIS and climate data. Ecol. Appl. 15 (3), 954–969.
Xie, X., Li, A., Jin, H., Tan, J., Wang, C., Lei, G., Nan, X., 2019. Assessment of five satellite-derived LAI datasets for GPP estimations through ecosystem models. Sci. Total Environ. 690, 1120–1130. https://doi.org/10.1016/j.scitotenv.2019.06.516.
Yoder, B.J., Pettigrew-Crosby, R.E., 1995. Predicting nitrogen and chlorophyll content and concentrations from reflectance spectra (400–2500 nm) at leaf and canopy scales. Remote Sens. Environ. 53 (3), 199–211.
Yuan, W., Cai, W., Xia, J., Chen, J., Liu, S., Dong, W., Wohlfahrt, G., 2014. Global comparison of light use efficiency models for simulating terrestrial vegetation gross primary production based on the LaThuile database. Agric. For. Meteorol. 192–193, 108–120. https://doi.org/10.1016/j.agrformet.2014.03.007.
Zhang, J., Sun, B., Yang, C., Wang, C., You, Y., Zhou, G., Xie, J., 2022a. A novel composite vegetation index including solar-induced chlorophyll fluorescence for seedling rapeseed net photosynthesis rate retrieval. Comput. Electron. Agric. 198, 107031 https://doi.org/10.1016/j.compag.2022.107031.
Zhang, Q., 2021. Characterization of a seasonally snow-covered evergreen forest ecosystem. Int. J. Appl. Earth Obs. Geoinf. 103, 102464.
Zhang, Q., Middleton, E.M., Cheng, Y.-B., Landis, D.R., 2013. Variations of Foliage Chlorophyll fAPAR and Foliage Non-Chlorophyll fAPAR (fAPAR $ _ {\rm chl} $, fAPAR $ _ {\rm non\mathchar" 702D chl} $) at the Harvard Forest. IEEE J. Sel. Top. Appl. Earth Obs. Rem. Sens. 6 (5), 2254–2264.
Zhang, Q., Xiao, X., Braswell, B., Linder, E., Baret, F., Moore III, B., 2005. Estimating light absorption by chlorophyll, leaf and canopy in a deciduous broadleaf forest using MODIS data and a radiative transfer model. Remote Sens. Environ. 99 (3), 357–371.
Zhang, Z., Li, X., Ju, W., Zhou, Y., Cheng, X., 2022b. Improved estimation of global gross primary productivity during 1981–2020 using the optimized P model. Sci. Total Environ. 838, 156172 https://doi.org/10.1016/j.scitotenv.2022.156172.
Zhao, L., Liu, Z., Xu, S., He, X., Ni, Z., Zhao, H., Ren, S., 2018. Retrieving the diurnal FPAR of a maize canopy from the jointing stage to the tasseling stage with vegetation indices under different water stresses and light conditions. Sensors 18 (11), 3965.
Zhao, M., Running, S.W., 2010. Drought-induced reduction in global terrestrial net primary production from 2000 through 2009. Science 329 (5994), 940–943. https://doi.org/10.1126/science.1192666.
Zheng, Y., Zhang, L., Xiao, J., Yuan, W., Yan, M., Li, T., Zhang, Z., 2018. Sources of uncertainty in gross primary productivity simulated by light use efficiency models: model structure, parameters, input data, and spatial resolution. Agric. For. Meteorol. 263, 242–257. https://doi.org/10.1016/j.agrformet.2018.08.003.